TSRR

IFAC-TSRR vol. 1 (2009) 129-140

Modeling the thermal response of the retina during Indocyanine Green-assisted peeling of the internal limiting membrane

Francesca Rossi([1]), Guido Toci([1]), Roberto Pini([1])
Fabrizio Giansanti([2]), Ugo Menchini([2])

([1]) IFAC-CNR, Via Madonna del Piano 10, 50019 Sesto Fiorentino, Italy
([2]) Dipartimento di Scienze Oto-Neuro-Oftalmologiche, Università di Firenze, Italy

INT.P07.001

 ISSN 2035-5831

1 - Introduction

The peeling of internal limiting membrane (ILM), has been recently introduced in macular hole surgery in order to assist hole closure [1-6]. Despite an increasing prevalence of ILM removal, the procedure is difficult to perform because of the poor visibility of the ILM. Various concentrations and types of Indocyanine Green (ICG) solutions have been used to stain and enhance the visibility of the ILM during macular hole surgery [7-11].

ICG is a water-soluble tricarbocyanine dye with a molecular weight of 775. Commonly used in ophthalmic surgery, it has a long history of safety after intravenous administration (e.g. to determine cardiac output, to test hepatic function and to visualize choroidal circulation) [12-17] despite some risk of toxicity to the outer retina especially at high concentrations, as reported in recent studies [18]. ICG has been also used as vital dye to stain the lens capsule in white cataract extraction [19].

However the safety of intravitreal use of ICG has not been proven yet. Recently, there have been studies describing ICG associated adverse effects in human eyes, such as retinal pigment epithelial atrophy and visual field defects possibly related to the use of ICG during intraocular surgery [20-24]. Other studies on animal eyes showed that ICG has toxic effects on the photoreceptors, retinal pigment epithelium and retinal ganglion cells [25-28]. On the contrary, other reports have demonstrated that the use of ICG to assist peeling of ILM in the macular hole surgery had no clinical evidence of ICG related retinal toxicity [8, 29].

The causes of retinal damage after ICG assisted ILM peeling are not yet completely clear. Previous studies have shown that different factors can participate in the ICG related retinal damage: type of solvent [27], osmolarity of solution,28 dose of ICG [29], time of contact of the tissue with ICG [30-32] and photo activation of ICG [33] by the light pipe causing a photodynamic effect.

As regard the mechanisms of action of photodynamic citotoxicity, two kinds of damage have been described: photo oxidation I, in which energy absorbed by the molecules can be converted into heat, damaging cells by raising their intracellular temperature; photo oxidation II, in which photosensitizer energy can be transferred to molecular oxygen forming a triple stage that interacts with oxygen to generate reactive intermediates, such as singlet oxygen [34, 35].

Another important aspect that in our opinion was worth investigating to assess the safety of ICG assisted ILM peeling was the possible development of heat side-effects in the retina caused by the direct absorption of light emitted by the vitrectomy instrument. In fact, as regards optical properties, ICG is a chromophore characterized by a strong optical absorption in the near infrared (the wavelength of the main absorption peak may vary depending on the type of solvent), and for this reason it is used in association with diode laser radiation to induce tissue welding in various types of tissue [36].

In the present work, we investigated the photothermal effect by developing a theoretical model which accounts for light absorption by ICG-stained ILM for the various spectral components of the Xenon lamp of the vitrectomy instrument. This model provides the thermal distribution induced into retinal structures, and makes it possible to calculate local temperature increase.

2 - Methods

To set up the thermal model, we used the typical ICG concentration and irradiation parameters employed for performing ICG-assisted peeling of the ILM in macular hole surgery. As reported in the literature, we assumed the use of purified iodine free ICG (Infracyanine®, Laboratoire SERB, Paris, France)

at a concentration of 0.25% [31]. In practice, 25 mg of sterile powder are dissolved in 5 ml of sterile isotonic 5% glucose solution; 5 ml of sterile balanced irrigating solution (BSS, Alcon, Fort Worth, TX) are added to produce the final solution.

A three-port vitrectomy is the routine approach. After *pars plana* vitrectomy has been performed, the ICG solution is injected over the posterior pole of the eye. The dye is left in place for 3 minutes and then removed with passive aspiration and then by BSS washing. Lastly, the peeling operation of the ILM is carried out, lasting for 5-10 minutes.

2.1 - Optical characterization of the problem

In order to study the light-induced heat processes during vitrectomy, the optical properties of the staining solution and the light source had to be investigated.

The absorption spectrum of Infracyanine® solution, prepared as described above, was measured by us using a JASCO spectrophotometer, Mod. V-560 (scanning speed of 100 nm/min, data pitch of 1 nm). The device was used in direct transmission of radiation throughout the sample, providing the spectral transmittance T. From T we derived μ_a , the absorption coefficient of the solution, being $T = \exp(-\mu_a d)$, where d is the path length of the light in the absorbing dye solution (see Fig. 1).

The emission parameters of a fiber illuminator (Optikon, mod. Sirius Xe, Rome, Italy), commonly used during vitrectomy, were measured. The illuminator included a Xenon discharge lamp as a primary light source. The spectrum of the lamp (see Fig. 2) was limited to the interval 400-700 nm, as the lamp emission was filtered before the coupling into the fiber by a UV-cutting filter and an IR-cutting filter. The maximum power emitted by a new, freshly clean fiber tip was 77.5 mW, as measured. This has to be considered as an upper limit, because the surgeon can reduce the power at his convenience and the fiber tip may become soiled during vitrectomy operations.

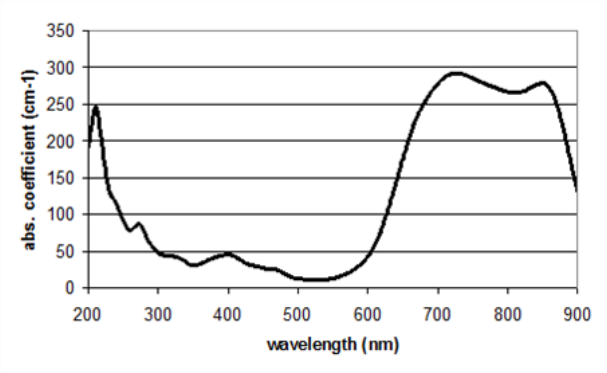

Fig. 1 - Absorption coefficient of the 0.25% Infracyanine® solution in glucose and BSS

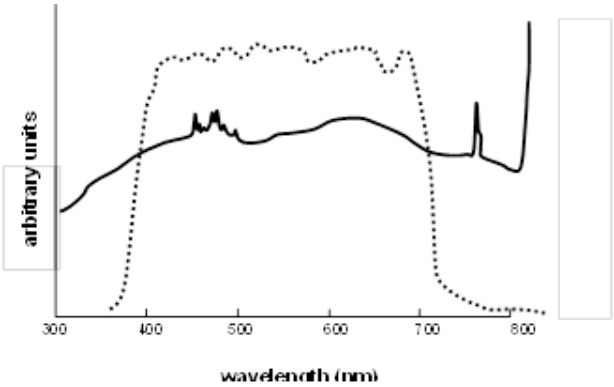

Fig. 2 - Emission spectrum of the Xe lamp (solid line) and transmission window after UV and IR filtering (dotted line)

The fiber diameter was D = 0.7 mm, and the lobe divergence in the vitreous or in the BSS filling the vitreous chamber was about α = 10°, half angle. The radius r_s of the spot impinging on the retina at a distance l from the fiber tip was then calculated from the expression $r_s = (D/2) + l \tan \alpha$.

2.2 - The theoretical thermal model

A simple bi-dimensional model of the eye was considered for describing the problem. The eye structure beneath the ILM was modeled with a sequence of plane layers of different thickness (see Fig. 3). The most superficial layer is the ILM, with a thickness of 5 μm [8], which absorbs part of the optical power due to the presence of the ICG dye, which provides local heating over a circular spot of radius r_s. The ILM is in thermal contact on one side with the BSS filling the vitreous chamber, which provides convection cooling, and on the other with the Neuroepithelium (NE), 500 μm thick [37], which is considered to be optically transparent. The NE is followed by the Retinal Pigment Epithelium (RPE), 10 μm thick [37], which absorbs another significant fraction of the impinging light, thus causing further heating. The underlying layers, down to a depth of several millimeters, were considered to have negligible optical absorption. The problem was assumed to have cylindrical symmetry around the axis of the illuminated spot, and was thus solved in the r-z plane, with r as the radial distance from the spot axis and z as the distance from the ILM surface. Light propagation is in the positive z-axis versus, i.e. from the vitreous chamber, filled with BSS, towards the retina.

To establish the temperature rise model, we considered a uniform temperature distribution of the eye at T = 37°C at time t = 0, when we turned on the illuminator and thus the heating in the ILM and in the RPE. We then studied the subsequent temperature rise. The modeled volume approximates an infinite medium along the r coordinate and a semi-infinite medium in the direction of positive z. This was realized with a cylindrical volume with a height of z = 7 mm and a radius r = 7 mm, with isothermal lateral and upper base surfaces (Dirichlet boundary condition) at temperature T = 37°C at z = 7 mm and at r = 7 mm. The upper surface of the cylinder (corresponding to the ILM surface) was considered to be in contact with the BSS filling the vitreous chamber, as we will discuss later.

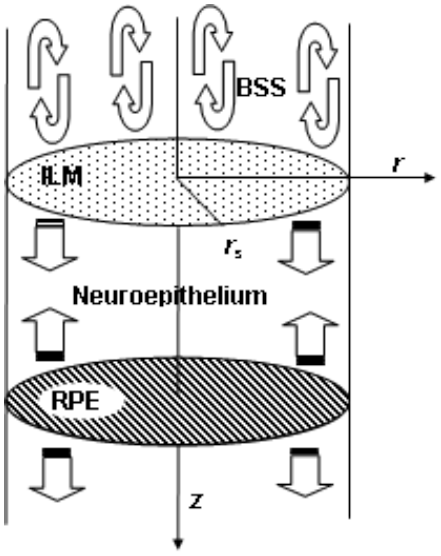

Fig. 3 - Schematic drawing of the eye model. Straight arrows indicate heating by conduction, while the curved ones heating by convection.

The governing differential equation for non-stationary heat propagation is:

$$\rho C \frac{\partial T}{\partial t} - \nabla(k \nabla T) = Q \tag{1}$$

The density ρ, heat capacity C and coefficient of heat conduction k were assumed to be the same in all the layers: respectively, ρ = 991.8 kg/m^3, C = 4067 J/(kg K), k = 0.63247 W/(m K) (i.e. the values for water at 37°C). The power deposited per unit volume Q in the ILM and in the RPE was evaluated as:

$$Q = PA/\left(\pi r_s^2 L\right) \tag{2}$$

where P is the overall power emitted by the fiber tip, A is the absorption either of the ILM or of the RPE, integrated in the 400-700 nm spectral interval, L is the layer thickness. We disregarded the exponential dependence of the deposited power density across the thickness of both ILM and RPE layers (and, therefore, its effect on the generated temperature profile across each layer), because of their relative thinness. The fraction of power transmitted beyond RPE was also neglected. The absorption of ILM due to the ICG was calculated using the absorption spectrum of Fig. 1 whereas for the RPE we used the absorption coefficint provided by Jacques and McAuliffe:[38]

$$\mu_{RPE}\left[cm^{-1}\right] = 6.49\times10^{12}\,\lambda\left[nm\right]^{-3.48} \tag{3}$$

We also considered the spectrum of the incident light on RPE to be already filtered by the upper ICG-stained ILM. With this model, it was found that about 3.4% of the incident power was absorbed by the ILM, and 80.2% was absorbed by the RPE.

The only heat transfer mechanism within the layers was assumed to be that of conduction. The convective cooling at the interface between the ILM and the BSS in the vitreous chamber was modeled as a heat flux:

$$F\left[W/m^2\right] = k\nabla T = -R\left(T_{ILM} - T_{BSS}\right) \tag{4}$$

(Neumann boundary condition) where T_{ILM} is the local temperature at the ILM surface, T_{BSS} is the temperature of the BSS in the vitreous chamber. The thermal resistance coefficient R was calculated as:

$$R = \left(Nu \cdot k\right)/r_s \tag{5}$$

where Nu is the Nusselt number calculated according to Raithby and Hollands [39] for a horizontal plate of radius r_s (i.e. the spot radius) cooled by natural convection in the semi-infinite water volume overlying the ILM. As R has slight dependence on (T_{ILM}-T_{BSS}), we used a value of R averaged over the temperature encompassed by the ILM surface. The values of R for various geometries are reported in Tab. 1. As a first step, T_{BSS} was assumed to remain constant at 37°C throughout the whole procedure and the model was developed considering only the heat processes in the retina.

As a second step, we assumed a more realistic situation considering the use of perfusion in the vitreous chamber: during vitrectomy, BSS at room temperature (25°C) is continuously injected into the eye. We thus simulated a convective flux in the vitreous chamber in front of the ILM surface, with the BSS having a starting temperature of 25°C. The heat flux between the ILM and the vitreous chamber was modeled as in (4), where T_{BSS} was calculated in the vitreous chamber model and the value of R was not averaged, but calculated in the simulation.

Simulation of the temperature rise in the eye tissues due to the illuminator was performed numerically by means of the Finite Element Method, implemented with a commercial software package (Femlab 3.0a, Comsol AB, Stockholm, Sweden).

3 - Results

The simulation modeled the temperature rise in the retina, due to the illumination of the ICG-stained ILM. The temperature profile was studied for 60 s after turning on the light on the ILM. The study was developed for several values of the spot radius (from 0.5 to 2 mm). A significant result of the simulation is reported in Fig. 4 (t = 60 s, spot radius = 1 mm).

In order to simplify calculations and reduce modeling time, symmetry considerations on the model geometry led to solve the problem in a semi-plane (r-positive plane), passing through the axis of the illuminated spot, and perpendicular to the ILM surface. The illumination propagated from negative z, and the zones with increasing z were located deeper and deeper under the ILM (see Fig. 3).

The buildup of the temperature distribution was rather fast, as can be seen in the graph of Fig. 5, which shows the temperature profile along z at $r = 0$ (i.e. along the symmetry axis) at various times after the beginning of the illumination.

Changing the spot radius (by changing the distance of the fiber tip from the retina) and the input power, the general shape of the temperature distributions was similar, but the peak temperature reached after 60 s by the RPE had a large variability. The results are summarized in Tab. 1.

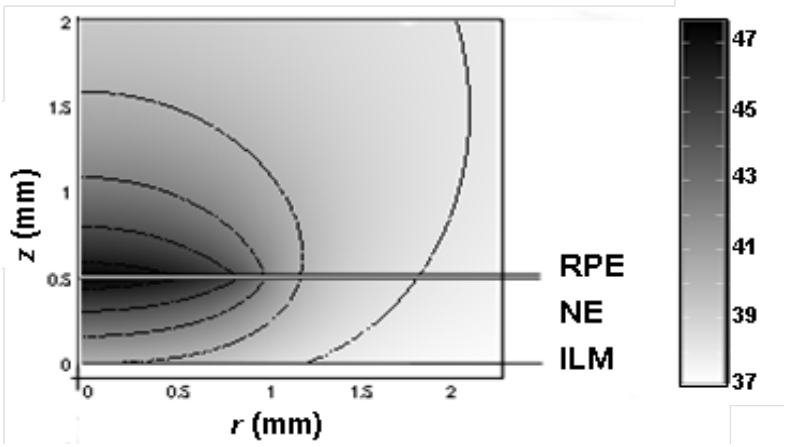

Fig. 4 - Temperature map in the retina at t = 60 s, induced by an incident power of 77.5 mW, emitted by the light pipe with a spot radius r_s of 1 mm on the ILM. The temperature in the ILM is 40.2°C, and in the RPE is 47.6°C. The gray levels are 1024, starting from 37°C.
The position of the various layers is also shown (the relative width of ILM and RPE is not in scale)

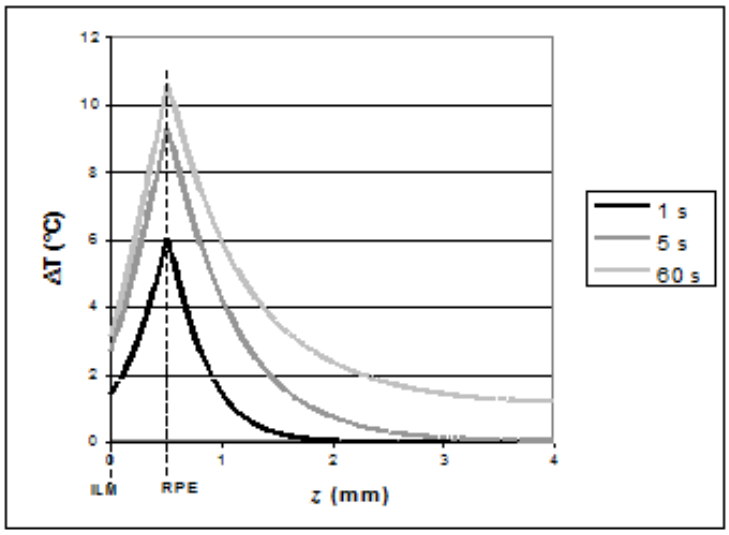

Fig. 5 - Distribution of the temperature increase from the initial value T = 37°C on the axis ($r = 0$) in the case of Fig. 4 at various times after illumination was begun. The temperature peak is situated in the RPE.

Tab. 1 - Simulation parameters and resulting maximum temperatures in the ILM and in the RPE

Spot radius r_s [mm]	Fiber distance l [mm]	Intensity [W/cm^2]	Thermal resistance R [W/(m^2 °C)]	T in ILM at t = 60 s [°C]	T in RPE at t = 60 s [°C]
0.5	0.85	9.87	4164	41.54	61.48
1	3.69	2.47	2792	40.16	47.57
1.5	6.52	1.10	1931	39.53	43.39
2	9.36	0.62	1708	38.86	41.31
1	3.69	0.95	2323	38.45	41.16

We can see that for very small spot radii the temperature increase in the RPE could be very great (more than 24°C for r_s = 0.5 mm). On the other hand, the temperature on the ILM surface remained rather low, due to the cooling effect of the BSS.

A simulation of illuminating the retina without staining the ILM was considered. It was noted that the presence of the ICG staining the ILM could provide some degree of protection to the RPE, in terms of thermal load and subsequent temperature rise. Indeed, the fraction of power that was absorbed near the surface of the ILM could readily be dissipated by thermal convection in the BSS, whereas the power absorbed in deeper layers (i.e. into NE and RPE) was dissipated through a conductive path which had a larger overall thermal resistance, and therefore induced a greater increase in temperature in the absorbing layer. The difference between stained and not-stained ILM were in the order of 0.1°C.

As described in the previous paragraph, we also simulated the case of perfusion, where BSS at an initial temperature of 25°C was injected into the vitreous chamber and convection motions were considered to calculate the temperature rise in both ILM and RPE. The cooling effects are thus more consistent, with respect to the previous case: for a spot radius of 0.5 mm, the temperature rise is about 17°C (it was 24°C in the previous case). The results are summarized in Tab. 2.

Tab. 2 - Simulation parameters and resulting maximum temperatures in the ILM and the RPE, considering perfusion in the vitreous chamber with BSS at 25°C and convection motions in the BSS

Spot radius r_s [mm]	Fiber distance l [mm]	Intensity [W/cm^2]	T in ILM at t = 60 s [°C]	T in RPE at t = 60 s [°C]
0.5	0.85	9.87	33.57	54.11
1	3.69	2.47	30.51	39.15
1.5	6.52	1.10	28.73	33.69
2	9.36	0.62	27.86	31.33

Moreover, to complete the picture, we also simulated a slightly different situation, which can occur in practical cases. In the previously considered model we have presumed that the surgeon can accomplish a perfect detachment between ILM and vitreous in actual operations. But occasionally the vitreous may not be completely detached.

We therefore supposed that the ILM remained covered by a thin layer (100 μm) of vitreous, stained with ICG. As expected, this layer was found to provide a more significant absorption of the incident light (as high as 38.8%) by using the ICG absorption curve of Fig. 1, so that only 54.1% of the incident light was absorbed by the RPE. The resulting temperature profile after 60 s of irradiation with an incident power 77.5 mW and a spot radius r_s = 1 mm, is shown in Fig. 6, curve (b).

By comparing this case (curve (b) of Fig. 6) with the case of same illumination parameters but without ICG (curve (a) of Fig. 6), we found that the effect of ICG staining was to effectively shield the RPE, producing a greater temperature rise below the irradiated surface, whereas in the RPE the temperature rise was lower. In numbers, the temperature in the ILM appeared to be to increased of 2.2 °C, while the temperature in the RPE was reduced of 2.4 °C.

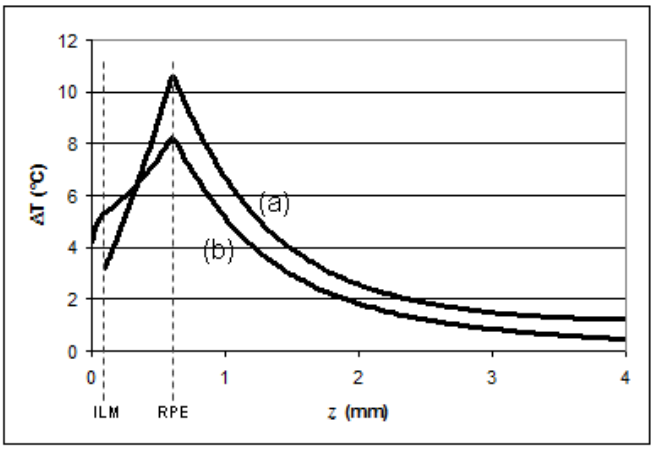

Fig. 6 - Temperature rise at t = 60 s, with a spot radius r_s = 1 mm, incident power of 77.5 mW.
Curve (a): without ICG.
Curve (b): case of a residual ICG-stained vitreous layer of 100 μm overlaying the ILM.

4 - Discussion

Ex vivo experiments were performed by different authors in order to study whether photoactivation of ICG induces[33] retinal damage or not[40] since this mechanism is not yet completely understood. The results of our simulation showed that the combination of ICG and light pipe illumination did not seem to cause important thermal changes in the ILM and in the RPE, compared to the use of the light pipe alone, as only 3% of the energy transmitted to the RPE was absorbed by the ICG-stained ILM.

We found that the temperature rise depended upon several parameters, such as distance of the fiber tip from the retina, emitting power of the light source, temperature of the BSS used as a perfusion in the vitreous chamber. It was noted that in some cases the temperature increase in the RPE could be significant, and the temperature peak was reached in about 20s after the light was turned on. On the other hand, the temperature increase in the ILM was found to be relatively modest, because only a small fraction of the incident intensity was absorbed in this layer, while the surface was cooled by the convection in the BSS. Convection played a prominent role in the dissipation of heat, a much more important one than that of the conduction toward deeper tissue layers. We found that the heat flux from the RPE to the ILM was about 50% greater than the one from the RPE toward deeper layers, as can be observed by the slope in the temperature profile (Fig. 5).

As was expected, excessive heating of the RPE could be avoided by increasing the distance between the tip of the light pipe and the retina, in order to obtain a larger spot radius with a lower incident power density, or, alternatively, by reducing the overall incident power (see line 5 in Tab. 1, where a lower illumination power set at 30 mW, with r_s = 1 mm, corresponding to a fiber distance of 3.7 mm, induced a temperature rise of 4.2°C in the RPE and of 1.5°C in the ILM).

It should be mentioned that other parameters can influence temperature variations in the retina with respect to those considered in our simulation. First of all, the degree of fundus pigmentation: melanosomes are responsible for the major quantity of absorption of energy emitted by the endoilluminator, but their concentration in the RPE can vary in different subjects. Moreover, the absorption curve of the ICG changes with concentration, solvent and pharmaceutical formulations,[41] thus changing the amount of absorbed light. In this work we used an ICG concentration of 0.25%, since some authors reported difficulties visualizing the ILM with lower concentrations.[42]

Worth noting is the cooling effect of the BSS: using a perfusion at room temperature (25°C) significantly reduces temperature values inside the retina. Only in the case of the smallest spot radius we considered (0.5 mm) and the maximum emitting power, a very high temperature in the RPE was found (see Tab. **2**).

Another question is whether the local blood flow in the choroid can play a significant role in the dissipation of the heat deposited in the retina. The choroid is situated just below the RPE, with a thickness of 180-250 μm, and covers about 85% of the internal eye surface, i.e. an area of about 1100 mm^2. The total blood flow perfusing the whole choroid is about 800 μl/min, i.e. 0.013 cm^3/s.[44] The volumetric blood flow

per choroid surface unit is thus $f = 1.24 \times 10^{-5}$ cm^3/(mm^2 s). The maximum power density which this blood flow can remove can be roughly estimated by assuming that the blood enters the irradiated spot at 37°C, and exits at the RPE peak temperature, with an overall temperature increase ΔT, being $P = C\rho f (\pi r_s^2) \Delta T$ the overall power removed by the choroidal blood flow. In the case exemplified in Fig. 4 (line 2 of Tab. 1, r_s = 1 mm, ΔT = 10.6°C), this power was about 1.7 mW. In case of line 4 of Tab. 1 (r_s = 2 mm, ΔT = 4.3°C), this power was about 2.3 mW, i.e. only a small fraction of the overall input power of 77.5 mW. The cooling capability of the choroid is therefore insufficient to compensate the thermal load imposed by the fiber illuminator.

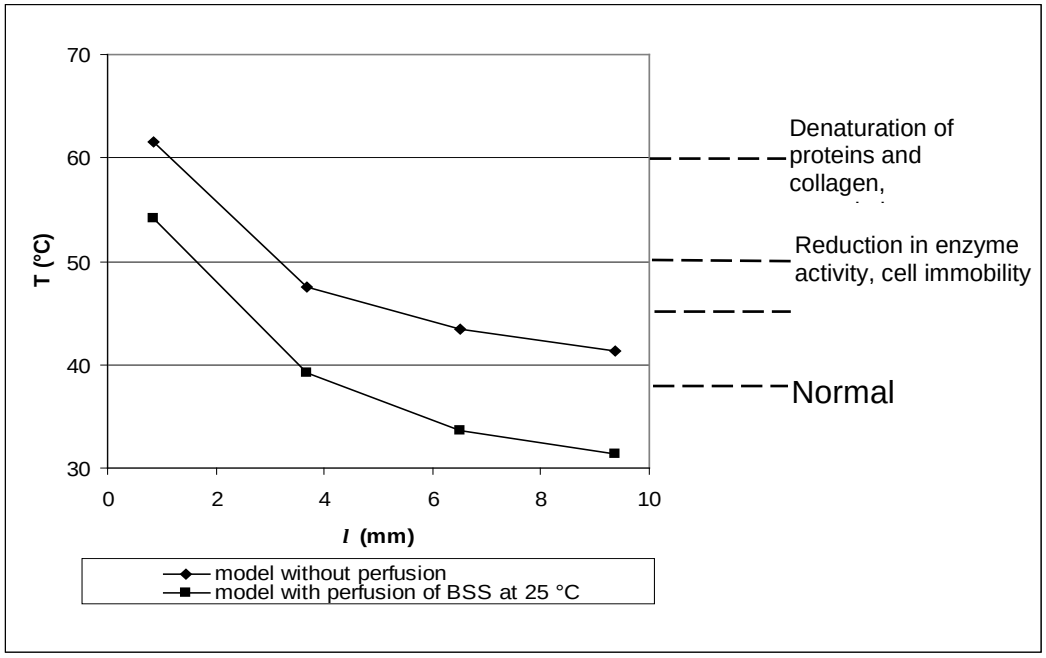

Fig. 7 - Calculated temperature values in the RPE for the models summarized in Tab. **1** (model without perfusion) and Tab. 2 (model with perfusion at T_{BSS} = 25°C). These values are compared with temperature inducing damages to biological tissues.[43]

The simulation of thermal damage to the tissue is summarized in Fig. 7. Considering that in actual cases the distance of the fiber tip from the retina is greater than 3-4 mm, we can observe that the most probable thermal damage is hyperthermia. This process is achieved at relatively low temperatures (42-50 ºC)[43] in mammalian cells, together with heat shock.[45,46] Mild heat shock inhibits DNA, RNA, protein synthesis, glycolisis and respiration.[45, 47] It induces cytoskeletal reorganization and heat shock protein synthesis in cells that have not sustained lethal damage. Heat shock kills mammalian cells by denaturing cellular proteins, damaging plasma membranes, and inactivating critical thermo labile molecular components.[45,47] Extensive intracellular protein denaturation occurs at temperatures above 43 ºC. The extent of thermal cellular injury depends on magnitude and duration of temperature increases to which the tissue is exposed (Arrhenius integral, thermal dose), and not on the total amount of energy deposited or the peak temperature experienced. [48-50] In hyperthermia, the effects produced by coagulation are absent if heat penetration is appropriately optimised.[51,52]

In previous works on the effect on the retina of ICG (0.05%) and illumination at certain wavelengths, Gandorfer et al.[33] demonstrated that severe damages to the cytoarchitecture of the inner retina may be induced. They revealed a regular retinal cytoarchitecture after illumination of the posterior pole with wavelengths between 380 and 760 nm when no ICG was used for staining of the ILM. The light pipe tip was placed 8 mm above the posterior pole for 3 minutes. If we compare those experimental results with our model, taking into account that we used different ICG concentrations, we can affirm that the temperature increase in the ILM and RPE is very little, using ICG or not.

In conclusion, considering the results of this thermal model, we can affirm that retinal damage during macular hole surgery is probably not caused by a purely thermal damage related to the use of highly-concentrated solutions of ICG: we found that ICG-stained ILM does not contribute to the temperature rise

in RPE. On the contrary it acts as a partial optical screen, reducing the fraction of light power which reaches the RPE by a few percent. In other words, if heat damage occurs, it is caused only by excessive light irradiation through the fiber illuminator. In such a case, the thermal damage is caused by hyperthermia, which depends on treatment time, light pipe tip distance from the retina, light power effectively emitted to the retina and temperature of the BSS used as a perfusion.

References

1. Park D.W.,. Sipperley J.O, Sneed S.R., et al., Macular hole surgery with internal limiting membrane peeling and intravitreous air, *Ophthalmology* 1999;**106**: 392-7.
2. Haritoglou C, Gass CA, Schaumberger M, Ehrt O, Gandorfer A,Kampik A. Macular changes after peeling of the internal limiting membrane in macular hole surgery. *Am J Ophthalmol*. 2001;132:363-368.
3. Brooks HL Jr. Macular hole surgery with and without internal limiting membrane peeling. *Ophthalmology*. 2000;107,1939-1948.
4. Mester V, Kuhn F. Internal limiting membrane removal in the management of full thickness macular holes. *Am J Ophthalmol*. 2000;129,769-777.
5. Kuhn F. To peel or not to peel, that is the question. *Ophthalmology*. 2002;109:9-11.
6. Hassan TS, Williams GA. Counterpoint: to peel or not to peel: is that question. *Ophthalmology*. 2002;109:11-12.
7. Burk Se, Da Mata AP, Snyder ME, Rosa RH Jr, Foster RE. Indocyanine green assisted peeling of the retinal internal limiting membrane. *Ophthalmology*. 2000;107:2010-2014.
8. Da Mata A.P., Burk S.E., Riemann C.D., et al., Indocyanine green assisted peeling of the retinal internal limiting membrane during vitrectomy surgery for macular hole repair, *Ophthalmology*. 2001; **108**: 1187-1192.
9. Kadonosono K, Itoh N, Uchio E, Nakamura S, Ohno S. Staining of internal limiting membrane in macular hole surgery. *Arch Ophthalmol*. 2000;118:1116-1118
10. Gandorfer A, Messmer EM, Ulbig MW, Kampik A. Indocyanine green selectively stains the internal limiting membrane. *Am J Ophthalmol*. 2001;131:387-388
11. Kusaka S, Hayashi N, Ohji M, Hayashi A, Kamei M, Tano Y. Indocyanine green facilitates removal of epiretinal and internal limiting membrane in myopic eyes with retinal detachment. *Am J Ophthalmol*. 2001;131:388-390.
12. Lund Johansen P. The dye dilution method for measurement of cardiac output. *Eur Heart J*. 1990;11(suppl):6-12
13. Leevy CM, Smith F, Longueville J, Paumgartner G, Howard MM. Indocyanine green clearance as a test for hepatic function. Evaluation by dichromatic ear densitometry. *JAMA*; 1967;200:236-240.
14. Flower RW, Hochheimer BF. A clinical technique and apparatus for simultaneous angiography of the separate retinal and choroidal circulations. *Invest Ophtahlmol*. 1973;12:248-261.
15. Hope Ross M, Yannuzzi LA, Gragoudas ES, et al. Adverse reactions due to indocyanine green. *Ophthalmology*.1994;101:529-533.
16. Guyer DR, Puliafito CA, Mones JM, Friedman E, Chang W, Verdooner SR. Digital indocyanine green angiography in chorioretinal disorders. *Ophthalmology*. 1992;99;287-291.
17. Yannuzzi LA, Slakter JS, SorensonJA, Guyer DR, Orlock DA. Digital indocyanine green videoangiography and choroidal neovascularization. *Retina*. 1992;12:191-223
18. J.E. Lee, T.J. Yoon, B.S. Oum, et al., Toxicity of indocyanine green injected into subretinal space: subretinal toxicity of indocyanine green, *Retina*, **23**, 675-681, 2003.
19. Horiguchi M, Miyake k, Ohta I, Ito Y. Staining of the lens capsule for circular continuous capsulorrexis in eye with white cataract. *Arch Ophthalmol*. 1998;116,535-537.
20. Haritoglou C, Gandorfer A, Gass CA, et al. Indocyanine green assisted peeling of the internal limiting membrane in macular hole surgery affects visual outcome: a clinicopathologic correlation. *Am J Ophthalmol*. 2002;134:836-841
21. Uemura A, Kanda S, Sakamoto Y, Kita H. Visual defects after uneventful vitrectomy for epiretinal membrane with indocyanine assisted internal limiting membrane peeling. *Am J Ophthalmol*. 2003;136:252-257.
22. Gass CA, Haritoglou C, Schaumberger M, Kampik A. Functional outcome of macular hole surgery with and without indocyanine green assisted peeling of internal limiting membrane. *Graefes Arch Clin Exp Ophthalmol*. 2003;241:716-720

23. Engelbrecht NE, Freeman J, Sternberg P Jr, et al. Retinal pigment epithelial changes after macular hole surgery with indocyanine green assisted internal limiting membrane peeling. *Am J Ophthalmol*. 2002;133:89-94
24. Hirata A, Inomata Y, Kawaji T, Tanihara H. Persistent subretinal indocyanine green induces retinal pigment epithelium atrophy. *Am J Ophthalmol*. 2003;136:353-355.
25. Iriyama A, Uchida S, Yanagi Y, et al. Effects of indocyanine green on retinal ganglion cells. *Invest Ophalmol*. 2004;45:943-947
26. Lee JE, Yoon TJ, Oum BS, Lee JS, Choi HY. Toxicity of indocyanine green injected into the subretinal space. *Retina*. 2003;23:675-681.
27. Ho DJ, Tsai RJF, Chen SN, Chen HC. Removal of sodium from solvent reduces retinal pigment epithelium toxicity caused by indocyanine green: implications for macular hole surgery. *Br J Ophthalmol*. 2004;88:556-559
28. Stalmans P, Van Aken EH, Veckeneer M et al. Toxic effect of indocyanine green on retinal pigment epithelium related to osmotic effects of the solvent. *Am J Ophthalmol*. 2002;134:282-285.
29. Sheidow TG, Blinder JK, Holekamp N, et al. Outcome results in macular hole surgery. An evaluation of internal limiting membrane peeling with and without indocyanine green. *Ophthalmology*. 2003;110:1697-1701.
30. Enaida H, Sakamoto T, Hisatomi T, Goto Y, Ishibashi T. Morphological and functional damage of the retina caused by intravitreous indocyanine green in rat eyes. *Graefes Arch Clin Exp Ophthalmol*. 2002;240:209-213.
31. Tadayoni R, Paques M, Girmens JF, Massin P, Gaudric A. Persistence of fundus fluorescence after use of indocyanine green for macular surgery. *Ophthalmology*. 2003;110:604-608.
32. Ciardella PA, Schiff W, Barile G, et al. Persistent indocyanine green fluorescence after vitrectomy for macular hole. *Am J Ophthalmol*. 2003;136:174-177.
33. Gandorfer A, Haritoglou C, Gandorfer A, Kampik A. Retinal damage from indocyanine green in experimental macular surgery. *Invest Ophalmol*. 2003;44:316-323
34. Abels C, Fickweiler S, Weiderer P, et al. Indocyanine green (ICG) and laser irradiation induce photooxidation. *Arch Dermatol Res*. 2000;292:404-411.
35. Baumler W, Abels C, Karrer S, et al. Photo-oxidative killing of human colonic cancer cells using indocyanine green and infrared light. *Br J Cancer*. 1999;80:360-363
36. McNally-Heintzelman K.M., Laser Tissue Welding, Chap. 39 in *Biomedical Photonics Handbook*, edited by T. Vo-Dinh, CRC Press, Boca Raton, 2003: 39-1/39-45.
37. Saraux H., Lemasson C., Offret H., Renard G., *La Retina, Anatomia e istologia dell'occhio*, 2nd ed. Milano, Masson Italia; 1982: 167-170
38. Jacques S. L., McAuliffe D.J., The melanosome: threshold temperature for explosive vaporization and internal absorption coefficient during pulsed laser irradiation, *Photochemistry and Photobiology*, 1991; **53**: 769-775.
39. Raithby G.D., Hollands K.G.T., in *Handbook of Heat Transfert Fundamentals 2nd ed.*, edited by W.M. Rosenhow, J.P. Hartnett, E.N. Ganic, McGraw-Hill, New York, 1985.
40. Grisanti S, Szurman p, Aisenbrey S, Oficjalska-Mlynczak J,Bartz-Schmidt KU. Histological findings in experimental macular surgery with indocyanine green. *Invest Ophthalmol Vis Sci*. 2004;45:282-286.
41. Haritoglou C., Gandorfer A., Schaumberger M., Tadayoni R., Gandorfer A., Kampik A., Light absorbing properties and osmolarity of indocyanine green depending on concentration and solvent medium. *Invest Ophthalmol Vis Sci*, 2003; 44:2722-2729.
42. Cheung B. T.O., Yuen C. Y.F, Lam D.S.C., Tang HM, Yan, Y.N, Chen W.U., ICG-assisted peeling of the retinal ILM, Letters to the Editor, *Ophthalmology*, 2002; 109(6): 1039-1040
43. Niemz H M. *Laser tissue interaction: fundamentals and applications*. Berlin, Springer-Verlag, 1996: 77-80.
44. see for example: *Ophthalmology*, chap. 8, edited by M. Yanoff, Mos publ., London, 1999
45. Lepock JR. Protein denaturation during heat shock. *Adv Molecular Cell Biol* 1997;19:223-259.
46. Field SB, Hand JW. Introduction to hypertermia. In Field SB, Hand JW, eds. An introduction to the practical aspects of clinical hyperthermia. New York: Taylor and Francis;1990:1-9
47. Dewey WC. Failla Memorial lecture. The search for critical cellular targets damage by heat. *Radiat Res*. 1989;120:191-204.
48. Birngruber R. Thermal modeling in biological tissues. In Hillenkamp F. Pratesi R. Sacchi CA, eds. Lasers in Medicine and Biology. New York, Plenum Publishing;1980:77-97.
49. Hall EJ. *Radiobiology for the Radiologist*. Philadelphia: J.B. Lippincott Company;1994.
50. Rol P, Fankhauser F, giger H, Durr U, Kwasniewska S. Transpupillar laser phototherapy for retinal and choroidal tumors; a rational approach. *Graefes Arch Clin Exp Ophthalmol*. 2000; 238:249-272

51. Burgess SEP, Chang S, Svitra P et al. Effect of hyperthermia on experimental choroidal melanoma. *Br.J Ophthalmol* 1985;69:854-860.
52. Coleman DJ, Silverman RH, Iwamoto T et al. Histopathologic effects of ultrasonically induced hyperthermia in intraocular malignant melanoma. *Ophthalmology* 1988;95:970-981.